

Contents lists available at ScienceDirect

BBA - Bioenergetics

journal homepage: www.elsevier.com/locate/bbabio



Binding of ferredoxin to algal photosystem I involves a single binding site and is composed of two thermodynamically distinct events^{*}



Pini Marco^a, Marina Kozuleva^a, Haviva Eilenberg^a, Yuval Mazor^b, Peter Gimeson^c, Andrey Kanygin^d, Kevin Redding^d, Iddo Weiner^a, Iftach Yacoby^{a,*}

- a School of Plant Sciences and Food Security, The George S. Wise Faculty of Life Sciences, Tel Aviv University, Ramat Aviv, Tel Aviv 69978, Israel
- ^b School of Molecular Sciences, Biodesign Institute Arizona State University, Tempe, AZ 85287-1604, USA
- ^c Malvern Instruments Limited, Enioma Rusiness Park, Grovewood Road, Malvern WR14, 1XZ, United Kinodom
- ^d School of Molecular Sciences, Center for Bioenergy & Photosynthesis, Arizona State University, Tempe, AZ 85287-1604, USA

ARTICLE INFO

Keywords: Photosystem I Ferredoxin Isothermal titration calorimetry Chlamydomonas reinhardtii Protein-protein interactions

ABSTRACT

Despite the impressive progress made in recent years in understanding the early steps in charge separation within the photosynthetic reaction centers, our knowledge of how ferredoxin (Fd) interacts with the acceptor side of photosystem I (PSI) is not as well developed. Fd accepts electrons after transiently docking to a binding site on the acceptor side of PSI. However, the exact location, as well as the stoichiometry, of this binding have been a matter of debate for more than two decades. Here, using Isothermal Titration Calorimetry (ITC) and purified components from wild type and mutant strains of the green algae *Chlamydomonas reinhardtii* we show that PSI has a single binding site for Fd, and that the association consists of two distinct binding events, each with a specific association constant.

1. Introduction

Oxygenic photosynthesis takes place in the chloroplast. In this dynamic landscape, large membrane-spanning protein complexes, such as photosystem I (PSI), interact with smaller proteins. PSI is an extremely efficient photoelectric apparatus, exhibiting a quantum efficiency of almost 100% [1]. The ability of PSI to convert sunlight energy to chemical energy is highly dependent on the precise spatial arrangement of the protein subunits and light harvesting complexes (LHC) as well as the relative positions of its cofactors. Also important is the proper interaction of PSI with external proteins such as plastocyanin (Pc) and ferredoxin (Fd). Among these various proteins, Fd is a soluble electron acceptor, reduced by PSI and located in the stromal area of the chloroplast [2]. Fd functions as an electron mediator, which distributes reducing equivalents from the light harvesting reactions to a variety of electron-dependent enzymes [3]. Still, notwithstanding the impressive progress made in recent years in understanding the structure [4] and early steps in charge separation within the photosynthetic reaction centers [5], our understanding of how ferredoxin interacts with the acceptor side of PSI is not as well developed. This lack of knowledge is particularly striking when one considers that Fd represents the sole link between the light reactions and critical downstream metabolic enzymes. The primary sink for reduced Fd is ferredoxin-NADP⁺ reductase (FNR), which generates NADPH. Other sinks are cyclic electron flow pathways, hydrogenase, sulfite reductase, nitrite reductase, thioredoxins, etc. [6, 7].

It is well established that Fd is directly reduced by the F_B cluster [8–10], bound by the PsaC subunit of PSI. Electron transfer (ET) to Fd occurs following a transient docking to the stromal ridge of PSI, which consists of the subunits PsaC, PsaD and PsaE [11–13]. However, the fine details of this binding event remain obscure. The affinity of Fd for PSI was extensively studied using flash absorption spectroscopy. Dissociation constant (K_d) values for *Chlamydomonas reinhardtii* around 6–9 μ M were determined [11–13]. For cyanobacterial PSI, a K_d range of 0.2–0.6 μ M was determined while a K_d of < 3 μ M was found for plant PSI [11, 12, 14]. In addition, these studies also pointed to the existence of more than one binding site, or different conformational states, for Fd on the stromal ridge of PSI, as evidenced by multiple kinetic components for reduction of Fd [14–16].

Following additional studies with cyanobacterial strains having point mutations in PSI stromal ridge subunits $[11,\ 12,\ 17,\ 18]$ and deletion strains of either PsaD or PsaE [19], a revised binding

E-mail address: iftachy@tau.ac.il (I. Yacoby).

^{*}Author contributions: P.M and I.Y: designed and performed research; M.K and H.E: performed research; Y.M and P.G: assistance in data analysis; A.K: contributed the mutant K35C; Iddo Weiner performed statistical analysis; All the Authors wrote the paper.

The authors declare no conflict of interest.

^{*} Corresponding author.

P. Marco et al. BBA - Bioenergetics 1859 (2018) 234–243

mechanism was proposed that involved electrostatic steering of Fd to PSI [13, 19]. In this binding process, non-specific electrostatic forces are responsible for the initial introduction between two protein molecules. Then, the proteins diffuse along each other through additional electrostatic forces until binding at the proper interface is achieved [20, 21]. Interestingly, while k'_{on} (the kinetic constant of complex formation) was substantially deteriorated in the absence of PsaD, only a small decrease was observed in the absence of PsaE; a reciprocal effect was observed for $k'_{\rm off}$ (the kinetic constant of complex dissociation). Based on these results it was proposed that PsaD affects the overall electrostatic steering of Fd into its binding site while PsaE mainly affects the lifetime of the complex [19]. This mechanism is also supported by the fact that PsaD is responsible for the increased affinity between Fd and PSI at pH 5.8, presumably through PsaD-His97. In summary, a steering mechanism could explain the multiple conformational states of Fd binding to PSI.

Use of flash absorption spectroscopy to observe the binding of Fd to PSI relies on the kinetics of Fd reduction by PSI. Consequently, sites not involved in ET would escape detection [22, 23]. Measurement of the $K_{\rm d}$ of the cyanobacterial Fd:PSI complex by backscattering interferometry, which does not rely on Fd reduction, was in quantitative agreement with previous work. For example, for cyanobacterial PSI, no evidence for a secondary binding site was found [23]. It was also observed that $Fd_{\rm 2Fe-2S}$ and $Fd_{\rm 2Ga-2S}$ (a synthetic form in which the iron atoms were replaced by Gallium) could not bind simultaneously to the cyanobacterial PSI, supporting a competitive model and making the possibility of two binding sites less probable [22].

The disagreement concerning the presence of two distinct binding sites for Fd on PSI is also reflected by the different structural models depicting the spatial contact between Fd and PSI. An earlier model placed cyanobacterial Fd at the side of the stromal ridge and in close contact with subunits PsaC, PsaD and PsaE [24]. This was revised in a model proposed by Ruffle et al. (2000) who studied two-dimensional crystalline arrays of cross-linked plant PSI:Fd complexes using electron microscopy. In this model, the binding of Fd to the stromal ridge of plant PSI is different than in the cyanobacterial PSI. A major difference is that Fd binding is observed on the top of the stromal ridge. In addition, in the plant cross-linked complex, the contact between Fd and PsaD was hardly detected, in stark contrast with the cyanobacterial complex [25].

In a later model, Jolley et al. (2005) addressed this discrepancy in a different way. They proposed the existence of two binding sites at the stromal ridge but with different affinities: a tight proximal one at the side and a looser distal one on the top [15, 26].

More support for the two binding sites hypothesis comes from the work by Lee et al. (2000). They used Kelvin force probe microscopy (KFM) for measuring electric potentials of the plant PSI stromal surface [27]. These experiments indicated peripheral docking of Fd ("side" or "proximal" according to [15, 24]) and light-induced movement to the central site of electron acceptance from F_B ("top" or "distal" according to [15, 25]).

In a more recent study by Cashman et al. (2014) computational approach based on the "frustration concept" [28] was employed for modeling potential Fd binding sites on the surface of cyanobacterial PSI [26]. This modeling effort yielded two docking pairs with opposite orientations. As a result, each docking pair had a different distance between the two nearest iron atoms of PsaC (F_B) and Fd. Such a difference may explain the different observations regarding the affinity and the energy transfer components seen between cyanobacteria, plant and algae.

In addition to the disagreement described so far, it was suggested that an evolutionary divergence took place, conferring organism-specific properties on the PSI:Fd:FNR super-complex [15, 25]. For example, although Fd and PSI from cyanobacteria, plant and algae interact with each other, the dissociation constants were different than in the homologous pair [14, 16]. It was also shown that FNR binds to PSI

through PsaE only in higher plants [29], enabling Fd to move directly towards FNR [15]. To our knowledge, there is no evidence for interaction of PsaE with FNR in cyanobacteria, although NADP + photo-reduction was shown to be dependent on PsaE in PsaE-less thylakoids from cyanobacteria [30]. The fact that cyanobacterial PSI interacts with phycobilisomes that are attached at the stromal side, [31] may hinder Fd from binding PSI at the distal site [25] and require Fd to diffuse away from PSI in order to interact with FNR [15].

Indication of multiple conformations/sites were also given by kinetic experiments in which NADPH or hydrogen production were measured by Ruffle et al. (2000) and Yacoby et al. (2011), respectively. Plant PSI:Fd cross-linked complexes were active only in the presence of soluble Fd, and the higher the Fd concentration used for cross-linking, the lower was the activity. This served as an indication for an additional binding site that was not bound by cross-linked Fd. This additional site may have a role in downstream ET to NADP⁺ [25]. A similar observation was reported by Yacoby et al. when Fd was fused to hydrogenase. In vitro this fusion enzyme was barely active, and addition of an excess of soluble Fd was a prerequisite for activity [32].

Isothermal titration calorimetry (ITC) is a technique for studying protein-protein interactions that directly measures the thermodynamic parameters of the binding events. In a typical experiment, the net change in heat released or absorbed by the system is recorded along a titration of a given macromolecule with its ligand. The dissociation constant (K_d), binding enthalpy (ΔH) and stoichiometry (N) are measured simultaneously in a single experiment [33–36]. Binding affinities of a few nM can be measured using ITC, obviating the need for labeling. However, large amounts of homogenous, stable and active binding partners are required [35, 37]. These requirements, together with the general heat sensitivity of membrane proteins, are challenging and limit studies with membrane proteins using ITC [35]. Indeed, to our knowledge there are only a few publications examining the binding properties of photosynthetic proteins using ITC. For example, the binding of several herbicides to photosystem-II was assessed using ITC [38]. Data from several studies exist for the interaction between Fd and FNR [34, 39, 40]. Most relevant, Fd binding to a heterologously expressed PsaD yielded a K_d of ${\sim}50\,\text{nM}$ [41], which was far lower than previously published K_d values measured for the Fd:PSI complex as a

Considering the controversial mechanism describing the binding of Fd to PSI, we desired to obtain further knowledge that will be required to refine the current models describing this crucial docking event. Therefore, in this work, we have performed a thorough ITC study of Fd binding to two active sub-populations of PSI (mature and immature) isolated from the model organism *C. reinhardtii*.

2. Materials and methods

2.1. Expression and purification of recombinant proteins

The recombinant proteins used in this study were heterologously expressed in *Escherichia coli* BL21 cells. Tobacco etch virus (TEV) protease expression plasmid, pMHTDelta238 was obtained from DNASU Plasmid Repository (dnasu.asu.edu/DNASU/Home.jsp). TEV protease expression procedure followed the auto-induction method [42] and purification was as previously described [43]. *C. reinhardtii* plastocyanin was prepared as described in [44].

The *C. reinhardtii* genes, petF (ferredoxin) and FNR, were cloned into pET21b vectors as fusions to maltose binding protein (MBP) with a 6xHis tag, separated by a linker (3xGGGGS) and TEV protease cleavage site (TEVc). Fd:TEVc:MBP:His6 and His6:MBP:TEVc:FNR *E.coli* cultures were grown in TB medium and induced by $50\,\mu\text{M}$ isopropyl $\beta\text{-}\text{D}\text{-}1\text{-}$ thiogalactopyranoside (IPTG, Formedium). For the induction of Fd, the culture was also supplemented with 1.25 mM ammonium ferric citrate (Sigma-Aldrich). Following expression, the fusion proteins were loaded on a HisTrap HP Ni²+ column (GE Healthcare) and eluted with 500 mM

P. Marco et al. BBA - Bioenergetics 1859 (2018) 234–243

imidazole (Sigma-Aldrich). Cleavage was performed by the addition of a 1:20 (w/w) amount of TEV protease (60 min, 34 °C). Then imidazole was removed using a desalting column (Centri Pure P25, emp Biotech). Cleaved Fd or FNR protein was flowed again through a HisTrap column; the column's flow through was collected as the product while MBP with His tag remained bound to the Ni column. Gel filtration chromatography (HiLoad 16/600 Superdex 200 prep grade column, GE Healthcare) was performed to separate the Fd and FNR from remaining TEV protease. Fd and FNR concentrations were determined spectrophotometrically according to the extinction coefficients $\Sigma_{422nm} = 9700 \, \text{M}^{-1} \, \text{cm}^{-1}$ for Fd [45] and $\Sigma_{458nm} = 10,700 \, \text{M}^{-1} \, \text{cm}^{-1}$ for FNR[46].

2.2. Algal strains growth and thylakoids preparations

Large quantities of highly pure photosystem I (PSI) are consumed in each ITC experiment. Therefore, C. reinhardtii strain JVD-1B[pGG1] [47] and its mutant derivative psaC:K35D [48], were chosen as these strains, having a His6-tag added to PsaA, enabled the production of large amounts of PSI. Cells were grown in TAP medium (Tris-acetatephosphate) at 25 °C with constant air flow under continuous white light (~70 μE) to late mid-log phase. The culture was harvested (4000 g, 5 min, 4 °C) and re-suspended in 30 mM Tricine-NaOH, 0.4 M sucrose, 15 mM NaCl (pH 7.7) buffer. Cells were disrupted by French press (1500 psi \times 3 rounds). Cells were centrifuged (6000g, 5 min, 4 °C) and a whitish pellet was separated from the disrupted cells in the supernatant. Membranes were harvested by centrifugation (110,000g, 60 min, 4 °C) and re-suspended in 20 mM Tricine-NaOH, 0.4 M sucrose, 150 mM NaCl (pH 7.7). Following a 30 min incubation, thylakoid membranes were precipitated again by centrifugation (110,000g, 30 min, 4°C) and resuspended in a minimal volume of 20 mM Tricine-NaOH, 0.4 M sucrose (pH 7.7) buffer. Chlorophyll (Chl) concentration was determined spectrophotometrically after extraction in 90% acetone according to [49]. Accordingly, Chl a/b ratio was calculated.

2.3. Isolation of PSI

PSI purification followed the protocols described in [47, 50]. Thy-lakoids were diluted to 0.8 mg Chl/ml in solubilization buffer: 25 mM Hepes-KOH, 100 mM NaCl, 5 mM MgSO₄, 10% glycerol (pH7.5), solubilized by the addition of 1/10 volume of 10% n-Dodecyl β -D-maltoside (DDM; Anatrace Inc.) and were gently mixed in the dark (30 min, 4 °C). Following centrifugation (46,000g, 25 min, 4 °C) the supernatant was loaded onto a HisTrap HP Ni²+ column pre-equilibrated with solubilization buffer +0.03% DDM and washed with the same buffer supplemented with 2 mM imidazole until UV absorbance reached a baseline. PSI was eluted by 1 column volume of 25 mM MES-NaOH, 100 mM NaCl, 5 mM MgSO₄, 10% glycerol, 0.03% DDM, 300 mM imidazole (pH7.0) buffer. The eluted PSI was loaded on sucrose density gradient tubes [50] made by freezing and thawing 0.65 M sucrose in 20 mM Tricine-NaOH, 0.03% DDM (pH7.7) buffer and separated by centrifugation (160,000g, 24 h, 4 °C).

2.4. SDS-PAGE

PSI complexes were analyzed by 15% SDS-PAGE (using Tris system) and stained by coomassie-blue.

2.5. Peptide mass spectrometry (MS)

PSI samples (in solution) were analyzed by MS in order to detect and compare the PSI subunits' composition in each PSI sample. Proteolysis: The proteins from the solution were extracted in 8M Urea. They were reduced with 2.8 mM DTT (60 °C for 30 min), modified with 8.8 mM iodoacetamide (in the dark, room temperature for 30 min) and digested with modified trypsin (Promega) at a 1:100 enzyme-to-

substrate ratio, overnight at 37 °C. An additional second digestion with trypsin was done for 4 h. Mass spectrometry analysis: The tryptic peptides were desalted using C18 tips (Home-made) dried and re-suspended in 0.1% Formic acid. The peptides were eluted with linear 30 min gradient of 5% to 28% acetonitrile with 0.1% formic acid in water, 15 min gradient of 28% to 95% acetonitrile with 0.1% formic acid in water and 15 min at 95% acetonitrile with 0.1% formic acid in water at flow rates of 0.15 μ l/min. Mass spectrometry was performed by a Q-Exactive plus mass spectrometer (Thermo) in a positive mode using repetitively full MS scan followed by High energy Collision Dissociation (HCD) of the 10 most dominant ion selected from the first MS scan. The mass spectrometry data was analyzed using the MaxQuant software 1.5.2.8 [51] vs. the *C. reinhardtii* proteome from the Uniprot database with 1% FDR. The data was quantified by label free analysis using the same software.

2.6. Determination of P_{700} concentration of the isolated PSI

An amount of PSI corresponding to 40 µg Chl was solubilized in 1 ml of 20 mM Tricine-NaOH, 10 mM ascorbate, 100 nM 2,6-dichlorophenol indophenol (DCPIP; Sigma-Aldrich), 10 nM Pc (pH 7.7) buffer, and placed in a quartz cuvette with a stirrer bar in the dark. By projecting the cuvette with saturating white light (Intralux 5000, Volapi) the reduced minus oxidized absorption difference in 700 nm was recorded spectrophotometrically (Cary 50, Varian). The particles were rereduced in the dark and photo-oxidized several more times (n = 9); the mean $\Delta A_{700 \text{nm}}$ was calculated. P_{700} (which corresponds to the reaction center of PSI) concentrations were determined by using an extinction coefficient of $100,000~\text{M}^{-1}~\text{cm}^{-1}$ [52]. Accordingly, Chl/P₇₀₀ ratio was determined for each PSI preparation (assuming all Chls are Chl a, Mw=893.5~g/mol).

2.7. NADP + photo-reduction activity assay

PSI at a final concentration of 30 nM was solubilized in 25 mM MES-NaOH, 100 mM NaCl, 5 mM MgSO₄, 0.03% DDM (pH 7.0) buffer supplemented with the following: $10 \, mM$ ascorbate, $50 \, \mu M$ DCPIP, $10 \, \mu M$ Pc, 5 µM Fd, 200 nM FNR and 1 mM NADP + (BioWorld). The mixture was placed in a quartz cuvette and measured using a Cary 50 spectrophotometer featuring a flash xenon lamp which makes its photomultiplier immune to ambient or actinic light. NADPH accumulation recorded spectrophotometrically using in 340 nm $(\Sigma = 6270 \,\mathrm{M}^{-1} \,\mathrm{cm}^{-1})$ by continuously projecting the cuvette with saturating white light (to compensate for the difference in antennae size between the two PSI forms) for 2 min. The activity was calculated as $\mu mol\ NADPH\ (1\ \mu mol\ PSI)^{-1}\ h^{-1}.$

2.8. Isothermal titration calorimetry (ITC)

PSI and Fd were concentrated by centrifugation (1500g, 4°C) in a filtering device (Amicon Ultra-15, 50,000 or 10,000 MWCO; Merck-Millipore) to the desired concentrations of 10-20 μM and 100-200 μM for PSI and Fd, respectively. Dialysis in a bag was performed in order to effectively match the buffers of PSI and Fd. The proteins were dialyzed (dialysis tubing cellulose membrane 14,000 MWCO, Sigma-Aldrich) against ×200 volumes of the experiment's buffer, in 4 °C while stirring in the dark for overnight. ITC experiments were carried out using the MicroCal PEAQ-ITC (Malvern) in a dark room. Fd, at 100-200 μM concentrations in the syringe, was titrated $(12 \times 3.2 \,\mu l$ injections) against 10-20 µM PSI in the ITC cell at 25 °C and a stirring speed of 750 rpm. In three experiments, 50 mM Hepes-KOH, 0.1% DDM (pH 7.5) buffer was used; 50 mM Tricine-NaOH and 25 mM sodium phosphate (0.1% DDM, pH 7.5) buffers were used once each. Also, two titrations were performed in 50 mM Hepes-KOH, 0.05% DDM (pH7.5) buffer supplemented with 5 mM MgCl₂. The data were fitted using a 'One Set of Sites' model or 'Two Sets of Sites' model or both (PEAQ-ITC Analysis

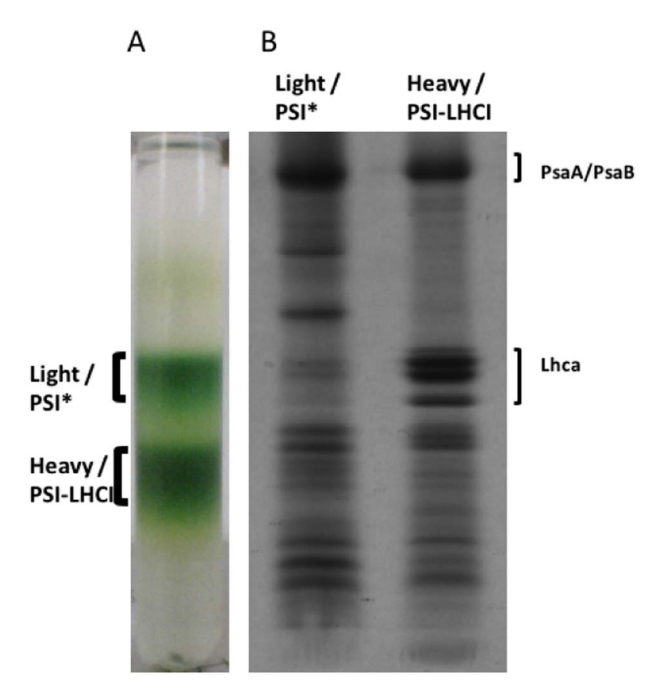


Fig. 1. Purification and evaluation of photosystem I. *Panel A*, sucrose density gradient showing the separation of PSI eluted from Ni²⁺ column to two sub-populations, PSI* and PSI-LHCI. *Panel B*, SDS-PAGE of PSI* and PSI-LHCI. Each lane was loaded with an amount of $1.3\,\mu\mathrm{g}$ Chl.

Software) as specified in the results section. The mean ΔH value from the three last injections was subtracted of all the data set to account for the heat of dilution. It should be elaborated that in order to avoid material loss or any other material downgrade, the ITC experiments were performed immediately following the purification-evaluation process.

3. Results

3.1. Isolation and evaluation of PSI particles

His-tagged PSI particles were purified from thylakoid membranes of the *C. reinhardtii* strain (JVD-1B[pGG1]) as previously described [47, 50]. The chlorophyll-containing eluates were loaded on a sucrose density gradient resulting in two populations of PSI with different densities (Fig. 1A "Light" and "Heavy"). SDS-PAGE analysis revealed several noticeable differences between the two PSI complexes (Fig. 1B). The most noticeable of these was the difference in antenna content. The light fraction contained considerably less Lhca proteins than the heavy fraction. Thus, we will refer to the heavy fraction hereafter as "PSI-LHCI".

Peptide mass spectrometry (MS) was used to assess the stoichiometry between PSI subunits relative to PsaA (Fig. 2). Each protein subunit is comprised of different peptides, upon trypsin proteolysis. These peptides are different in their numbers, lengths and spectral intensities. Thus, one cannot expect a 1:1 stoichiometry for each of the subunits although the intensities were normalized to the molecular weight of the protein subunit. A difference between the two PSI forms should indicate whether a subunit is present or absent in the preparation

This MS analysis (Fig. 2 and Table 1) revealed that most PSI subunits (PsaA,B,C,D,E,H,L) were present in both types of PSI complexes, as the relative amounts were comparable between the two PSI forms. As expected, PsaI, PsaJ, PsaN and PsaO were not identified by MS as previously reported [50]. PsaF, PsaG and PsaK relative values in the light form were lower than those in PSI-LHCI ($p \le .05$ in a 1 tailed t-test). Also, all 9 Lhca proteins relative amounts were significantly lower

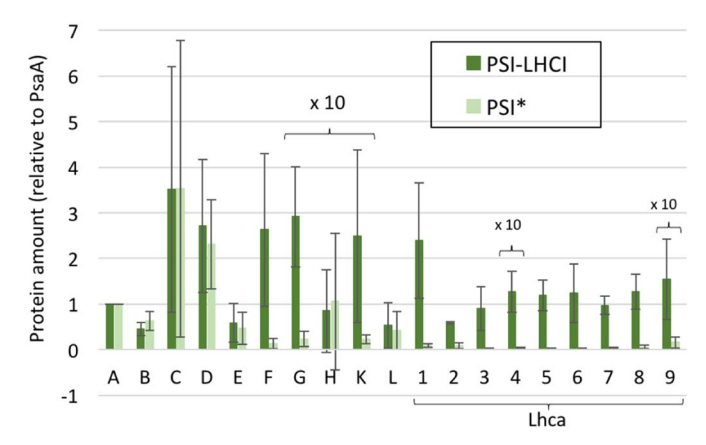


Fig. 2. Determination of the amount of individual subunits relative to PsaA by peptide MS. The spectral intensities were normalized once with the molecular weight of the subunit and another time against the amount of PsaA in that sample. PSI-LHCI and PSI* relative amounts of PsaB,C,D,E,H and PsaL subunits were comparable. PsaF, PsaG and PsaK relative protein amounts were much lower in PSI* preparation. Also, all 9 Lhca proteins were present in PSI-LHCI preparations, while for PSI* their spectral intensities could hardly be detected. Data shown is mean \pm SE (n = 3). Some of the values were multiplied by factor of 10 for convenience. The values are presented in Table 1.

Table 1 Amounts of PSI subunits relative to PsaA measured by peptide MS. Data shown is mean \pm SE (n = 3).

| Subunit | PSI-LHCI | PSI* |
|---------|----------------|-----------------|
| PsaA | 1.0 | 1.0 |
| PsaB | 0.5 ± 0.1 | 0.6 ± 0.2 |
| PsaC | 3.5 ± 2.7 | 3.5 ± 3.3 |
| PsaD | 2.7 ± 1.5 | 2.3 ± 1.0 |
| PsaE | 0.6 ± 0.4 | 0.5 ± 0.3 |
| PsaF | 2.6 ± 1.7 | 0.1 ± 0.1 |
| PsaG | 0.3 ± 0.1 | 0.02 ± 0.02 |
| PsaH | 0.1 ± 0.1 | 0.1 ± 0.1 |
| PsaK | 0.3 ± 0.02 | 0.02 ± 0.01 |
| PsaL | 0.5 ± 0.5 | 0.4 ± 0.4 |
| Lhca1 | 2.4 ± 1.3 | 0.1 ± 0.05 |
| Lhca2 | 0.6 ± 0.02 | 0.1 ± 0.1 |
| Lhca3 | 0.9 ± 0.5 | 0.02 ± 0.02 |
| Lhca4 | 0.1 ± 0.04 | n.d |
| Lhca5 | 1.2 ± 0.3 | 0.02 ± 0.01 |
| Lhca6 | 1.2 ± 0.6 | 0.02 ± 0.01 |
| Lhca7 | 1.0 ± 0.2 | 0.03 ± 0.02 |
| Lhca8 | 1.3 ± 0.4 | 0.1 ± 0.04 |
| Lhca9 | 0.2 ± 0.1 | 0.02 ± 0.01 |
| | | |

in the light form (p < .05 in a 1 tailed t-test). This indicate that most of the light PSI particles were missing PsaF/G/K subunits and all 9 Lhca. Therefore, the light fraction hereafter will be referred to as "PSI*" in accordance with [53].

The pigment content of both particles was consistent with the loss of Lhca antenna from the PSI* preparation. The mean Chlorophyll per P_{700} was 305 \pm 55 (n = 15) and 106 \pm 13 (n = 11) for PSI-LHCI and PSI*, respectively. Moreover, the mean Chl a/b ratio was 5.7 \pm 0.6 (n = 11) and 24 \pm 9.9 (n = 6) for PSI-LHCI and PSI*, respectively. This observation is in line with a reduced content of *C. reinhardtii* antenna complexes within PSI* [50], as the core antenna of PSI (100 Chl a) contains no Chl b; Thus, only LHCI contributed Chl b to the associated antenna pigment pool [4]. These marked differences between the two PSI populations clearly indicate that PSI* is an immature form of PSI, lacking not only the peripheral antenna but some of core subunits. This observation is in line with the suggestion of Ozawa et al. (2010) that PsaG and PsaK are the last subunits to be incorporated during the PSI assembly process and have a structural role in capping the antenna complexes [54].

Since there are numerous factors which govern the proper assembly

P. Marco et al. BBA - Bioenergetics 1859 (2018) 234–243

of the holo PSI-LHCI complex, one cannot predict that a given complex is functional just by evaluating SDS-PAGE or the photo-reduction rate of oxygen by PSI in the presence of methyl viologen, an artificial electron acceptor. Therefore, we assayed the complete electron transport chain of PSI using the native electron acceptors. For that aim, we measured the NADPH photo-production rate of purified PSI in the presence of Fd and FNR under saturating light (1000 µE (m² sec)⁻¹). The kinetic photo-reduction assay was carried out using a reconstituted ET chain system, with ascorbate serving as the ultimate electron donor together with soluble electron mediators. PsaF is known to be important for the docking of plastocyanin (Pc) [55, 56] in C. reinhardtii and other eukarvotes. Since it was missing from PSI* preparations, either the electron mediators Pc or 2.6-dichlorophenol indophenol (DCPIP) were used as electron mediators to PSI. Fd is initially reduced by PSI and then binds and reduces FNR, which in turn catalyzes NADP+ reduction. In the presence of Pc, PSI-LHCI (142 \pm 55 μ mol NADPH (μ mol PSI)⁻¹ h⁻¹, n = 5) was more active than PSI^* (9.7 \pm 6 NADPH (µmol PSI)⁻¹ h⁻¹, n = 5). In the absence of Pc, the rates were generally lower $(3.74 \pm 0.32 \text{ and } 1.06 \pm 0.03 \,\mu\text{mol NADPH/(}\mu\text{mol PSI)}^{-1} \,\text{h}^{-1} \,\text{for}$ PSI-LHCI and PSI*, respectively; n = 3) since DCPIP is a less efficient donor. The fully mature PSI-LHCI was 14-fold more active than PSI* with Pc as electron donor, and 3.5-fold more active with DCPIP alone. This result indicates that it is the plastocyanin docking site, which is presumably impaired in PSI*. Indeed, an acceleration in re-reduction of photo-oxidized P₇₀₀ + in response to Pc addition was observed only for PSI-LHCI P_{700} (0.09 \pm 0.004 s⁻¹ and 0.44 \pm 0.04 s⁻¹ with Pc) but not for PSI* $(0.1 \pm 0.001 \,\mathrm{s}^{-1})$ and $0.14 \pm 0.007 \,\mathrm{s}^{-1}$, n = 3), as presented in Fig. S1.

3.2. ITC studies

Since our analysis revealed defects in the ability of PSI* to interact with both electron donors and acceptors, we used ITC to study the binding of Fd to both preparations of PSI in order to gain more insight into the origin of these functional differences. ITC can be used to measure dissociation constants as low as 5–10 nM [37]. During an experiment, the change in the total heat of the system is recorded and seen as peaks, corresponding to each injection of the ligand. Thus, ITC peaks comprise not only the binding event, but any process resulting in heat lose/gain, including dilution of the proteins during titration, mix of disparate buffers in the syringe and the ITC cell and ion exchange between the solvent and the complex. All these factors can affect the measurements. To address this issue in our procedure, a few preliminary experiments were conducted.

The efficiency of our dialysis procedure in matching our detergent containing buffers was tested. Detergents are not easily dialyzed [35, 57] and thus a minor difference between the solvents could take place. In the first control experiment, two post-dialysis blank solutions were mixed in the ITC device as in a typical experiment. Weak negative peaks (exothermic heat change) in the range of -0.43 ± 0.15 kcal/mol were generated (Fig. S2) in contrast to the positive peaks (endothermic) observed for Fd:PSI binding (Fig. 3), which were in the range of \sim 3.0 \pm 0.5 and \sim 1.0 \pm 0.1 kcal/mol for PSI-LHCI and PSI*, respectively. Thus, the contribution from buffer mismatch is negligible. To assess the heat generated during the dilution of Fd as well as that of PSI in the ITC cell, two additional control experiments were conducted; blank dialysis buffer in the ITC cell was titrated with Fd, and PSI in the cell was also titrated with a blank buffer, as in a typical ITC experiment. in (Fig. S3, $-0.41 \pm 0.08 \, \text{kcal/mol};$ $0.07 \pm 0.06 \, \text{kcal/mol}$), both experiments resulted in weak heat signals, approving that any contribution from the dilution of Fd and/or PSI would be negligible. Thus, the validity of the ITC procedure was supported by these results.

3.3. PSI-LHCI vs. Fd

Fig. 3A presents a typical experiment in which Fd was titrated into a sample cell containing PSI-LHCI (see Fig. S5 for additional repeats). Each injection of Fd into the cell generated an endothermic heat signal (positive peaks). Following the recording of the heat changes, PEAQ-ITC Analysis Software was used to fit the raw data according to the 'Two Sets of Sites' model. Fig. 3A shows a typical bi-phasic binding curve, recorded at pH7.5, which indicates that two binding events have occurred, each with a defined enthalpy. The first event binding curve showed maximum inflection at Fd:PSI ratio of 0.5. The latter step of the binding curve represents the second binding event that showed maximum inflection at Fd:PSI ratio of 1.0. Accordingly, the overall stoichiometry is 1:1. It should be emphasized that the use of the word 'event' in the text is in the simple meaning of an occurrence, and isn't to imply any chronological order to these binding events.

Table 2 (lines 1–3) shows the binding parameters obtained from three independent experiments using Hepes at pH 7.5. Mean stoichiometry values, N, of 0.49 \pm 0.01 and 0.97 \pm 0.02 were obtained for the first and second binding events, respectively. Hereafter they will be referred to as 'event I' and 'event II'. For both binding events the positive enthalpy component, $\Delta H_{\rm h}$ is unfavorable to the negative free energy, $\Delta G_{\rm h}$ and the entropy contribution, $-T\Delta S_{\rm h}$ drives the two reactions.

Event I affinity, K_d of 29 \pm 12 nM, was larger than that of event II, K_d of 247 \pm 14 nM. The affinity of Fd for PSI depends on both NaCl and MgCl₂ concentrations, but the largest affinity at pH 8.0 was observed in the presence of 5 mM Mg²⁺ and in the absence of NaCl [16]. Titrations in the presence of 5 mM Mg²⁺ resulted with similar N and K_d values, but the ΔH was higher for both events (Table 2 and Fig. S5).

Exchange of protons between ionizable groups in any of the binding partners and the bulk solvent results in a contribution to the measured binding enthalpy change from ionization of the buffer [40, 58]. In order to examine whether protons are exchanged during Fd:PSI binding process we used both phosphate and Tricine as alternative buffers at pH 7.5. Fig. 4 and Table 2 show that exchanging buffers from Hepes to either Tricine or phosphate resulted in an increased $K_{\rm d}$ (p < .05) only for event II. This indicates that the two binding events are distinct (for ITC experiments with Tricine and phosphate buffers, see Fig. S6).

Buffer exchange specifically changed the enthalpy of binding in event I (ΔH_{I}), while ΔH_{II} was not significantly affected (Table 2). As can be seen in Fig. 5 the higher the intrinsic buffer ionization enthalpy (ΔH_{ion}) the lower was ΔH_{I} . It is well documented [40, 58, 59] that linear regression of the binding enthalpy values reveals the number of protons exchanged between the protein complex and the solvent (n_{H+}) , and ΔH^0 , which is the buffer-independent binding enthalpy. Hence, the calculated slope of -0.57 indicates a net de-protonation of ~ 0.6 protons, on average, between ionizable groups and the bulk solvent in event I, while no such proton exchange occurs during event II. The intercept at 7.3 kcal/mol equals ΔH_I^0 , i.e. the enthalpy of Fd binding during event I minus the heat of ionization from proton release. This value is closest to $\Delta H_{I(phosphate)}$ for which the lowest ionization enthalpy contribution was observed ($\Delta H_{ion(phosphate)} = 1.22 \, kcal/mol$). In contrast, $\Delta H_{\rm II}$ was not affected by the buffer exchange, as can be seen from nearly invariant values of binding enthalpy (Fig. 5). These energetic differences between the binding events support the existence of two distinct PSI:Fd binding modes.

3.4. PSI* vs. Fd

As presented above, PSI* is an immature form of PSI, which was also characterized by a lower rate of NADP⁺ photo-reduction. This suggests that the binding properties of Fd to PSI* will be affected. Fig. 3B presents a typical experiment in which Fd was titrated into a PSI* containing sample cell (see Fig. S8 for additional repeats). At pH 7.5 a conventional sigmoid binding curve was observed, consistent with a

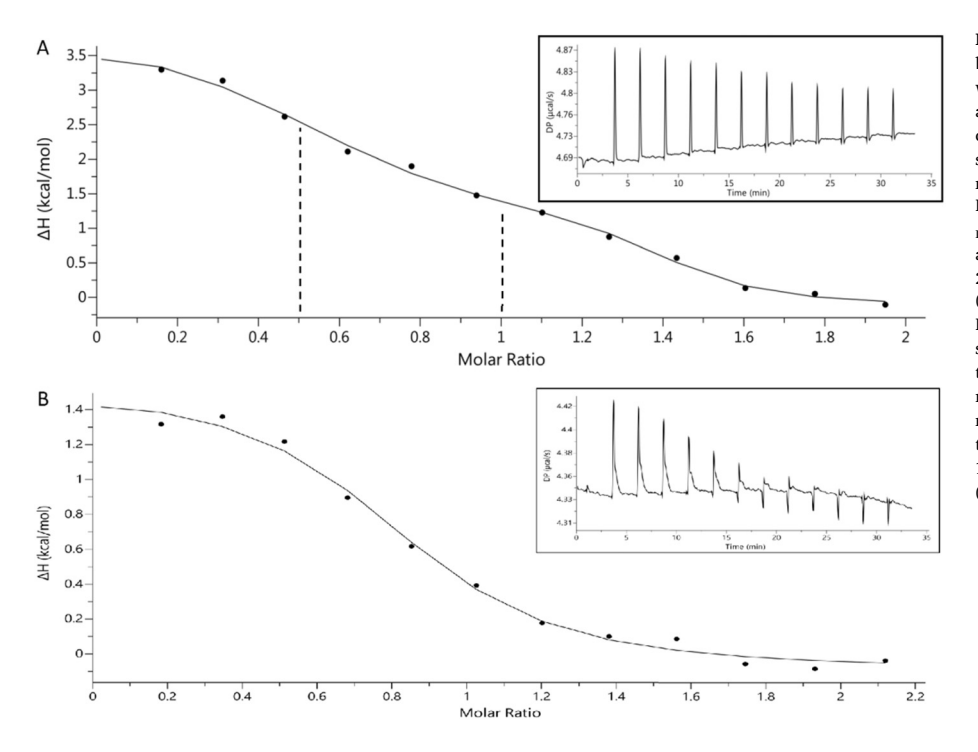


Fig. 3. Panel A. titration of PSI-LHCI with Fd in Hepes buffer. The raw heat changes peaks (inset) were subtracted with the average value of the last three injections and fitted according to a two sets of sites model. The resulted binding curve is bi-phasic showing two events of a single binding site: the first event shows maximum inflection at Fd:PSI molar ratio of \sim 0.5 and the second at \sim 1.0 (dotted lines). Binding at the first event, event I, was characterized by a K_d $_{\rm I}$ of 29 \pm 12 nM and $\Delta H_{\rm I}$ of 4.43 \pm 0.28 kcal/mol. Binding at the second event, event II, was characterized by a $K_{d\ II}$ of $247 \pm 14 \, \text{nM}$ and ΔH_{II} of $1.21 \pm 0.17 \, \text{kcal/mol}$ (value + SE, n = 3), Panel B, titration of PSI* with Fd in Hepes buffer. The raw heat changes peaks (inset) were subtracted with the average value of the last three injections and fitted according to a one set of sites model. The resulted binding curve is a conventional sigmoid and shows maximum inflection at Fd:PSI molar ratio of 0.8. Binding at this single event was characterized by a K_{d PSI₂} of $1.5\,\pm\,0.34\,\mu M$ and ΔH_{PSI_*} of $1.74\,\pm\,0.07\,kcal/mol$ (value \pm SE, n = 3).

Table 2
Thermodynamic parameters of PSI-LHCI:Fd binding from ITC experiments.

| Buffer in use | | Binding event I | | | | Binding event II | | | | | |
|--------------------------|-----------------|--------------------------|-------------------------|-------------------------------|-------------------------------|----------------------------------|--------------------------|------------------------|--------------------------------|--------------------------------|-----------------------------------|
| | | N _I (sites) | K _{d I} (nM) | ΔH _I (kcal/mol) | ΔG _I (kcal/mol) | - TΔS _I (kcal/mol) | N _{II} (sites) | K _{d II} (nM) | ΔH _{II} (kcal/mol) | ΔG _{II} (kcal/mol) | – TΔS _{II} (kcal/mol) |
| Hepes | 1.ª | 0.48 | 25.2 | 4.07 | -10.4 | -14.4 | 0.89 | 245 | 1.27 | -9.02 | -10.3 |
| | 2. ^b | ± 0.02 0.48 ± 0.01 | ± 8.1 30.8 ± 15.3 | ± 0.16 4.73 ± 0.41 | -10.2 | -15.0 | ± 0.03 1.01 ± 0.01 | ± 23 231 ± 7 | ± 0.12 1.20 ± 0.29 | -9.05 | -10.3 |
| | 3. ^b | 0.51 ± 0.02 | 30.5 ± 11.1 | ± 0.41 4.49 ± 0.26 | -10.3 | -14.8 | 1.02 ± 0.02 | 265 ± 11 | ± 0.29 1.15 ± 0.11 | -8.97 | -10.1 |
| Mean (Hepes) | | 0.49 ± 0.01 | 29.0 ± 12 | ± 0.26 4.43 ± 0.28 | -10.3 | -14.7 | 0.97 ± 0.02 | 247 ± 14 | ± 0.11 1.21 ± 0.17 | -9.01 | -10.2 |
| Hepes + Mg ²⁺ | 4. ^c | 0.47 ± 0.03 | 17.6 ± 5.1 | 9.0 ± 0.34 | -10.6 | -19.6 | 1.02 ± 0.03 | 280 ± 23 | ± 0.17 4.89 ± 0.21 | -8.95 | -13.8 |
| | 5.° | 0.56 ± 0.05 | 15.7 ± 13.1 | 7.75 ± 0.34 | -10.7 | -18.4 | 1.02 ± 0.03 | 250 ± 9 | ± 0.21 4.06 ± 0.21 | -9.02 | -13.1 |
| Tricine | 6. ^d | 0.56 ± 0.05 | 18.8 ± 7.3 | ± 0.34 2.89 ± 0.07 | -10.5 | -13.4 | 0.90 ± 0.03 | 469 ± 32 | ± 0.21 1.49 ± 0.07 | -8.64 | -10.1 |
| Phosphate | 7. ^e | 0.39 ± 0.05 | ± 7.3 17.2 ± 2.2 | ± 0.07 6.57 ± 0.16 | -10.6 | -17.2 | 0.92 ± 0.02 | ± 32 482 ± 14 | ± 0.07 1.84 ± 0.1 | -8.62 | -10.5 |

 $[^]a$ 10.6 μM PSI-LHCI vs. 100 μM Fd in 50 mM Hepes-KOH, 0.1% DDM.

single binding event. The curve's maximum inflection was not at Fd:PSI ratio of 1.0, as would have been expected. Since this event corresponds to the only binding event for this PSI population, and this complex is active in ET to Fd, as evidenced by the NADP $^+$ photo-reduction assay, it was named "event PSI*". For this event, we measured a stoichiometry of 0.8 \pm 0.02, a dissociation constant, $K_{d\ PSI_*}$ of 1.5 \pm 0.34 μM , and a binding enthalpy of $\Delta H_{PSI_*}=1.74~\pm~0.07$ kcal/mol (n = 3). Similar to both binding events observed for PSI-LHCI, the binding between Fd to PSI* generated endothermic heat signals and a total positive ΔH (mean $\Delta G=-7.9$ kcal/mol, $-T\Delta S=-9.7$ kcal/mol), suggesting that this interaction is entropy driven by nature. Furthermore, $K_{d\ PSI_*}$ was sixfold higher than $K_{d\ II}$ of PSI-LHCI, reflecting a lower affinity of PSI* for Fd. The values of ΔH_{PSI_*} and ΔH_{II} (1.74 and 1.21 kcal/mol, respectively)

are somewhat similar, implying that event PSI* and event II are related and perhaps represent largely the same event.

3.5. PsaC K35D mutant PSI vs. Fd

A single mutation in PsaC, K35D, where a lysine was exchanged for an aspartic acid. $\,$

is known to cause a dramatic decrease in affinity of binding between Fd and PSI [11, 12]. In order to validate our results, we examined the interaction between Fd and PSI complexes isolated from a strain carrying the PsaC-K35D mutation. As seen in Fig. 6, this mutation completely abrogated all the heat signals corresponding to Fd:PSI-LHCI binding in our assay. We conclude that event I and II involved in

 $[^]b$ 12 μM PSI-LHCI vs. 120 μM Fd in 50 mM Hepes-KOH, 0.1% DDM.

 $[^]c$ 7.0 μM PSI-LHCI vs. 70 μM Fd in 50 mM Hepes-KOH, 0.05% DDM, 5 mM MgCl $_2$

 $^{^{\}rm d}$ 11.7 μM PSI-LHCI vs. 120 μM Fd in 50 mM Tricine-NaOH, 0.1% DDM.

 $^{^{}e}$ 19.3 μM PSI-LHCI vs. 193 μM Fd in 25 mM sodium phosphate, 0.1% DDM.

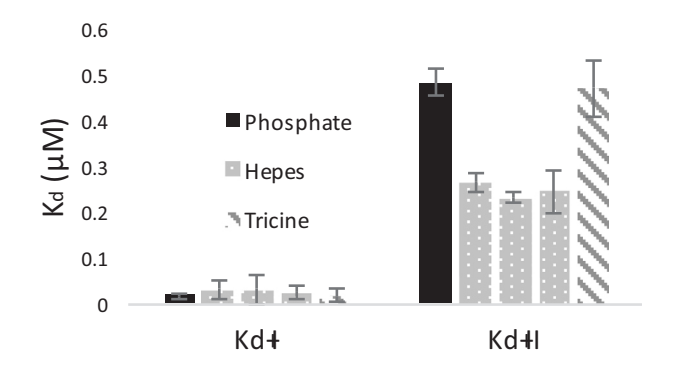


Fig. 4. Buffer effect on $K_{d~I}$ and $K_{d~II}$ of PSI-LHCI:Fd binding. The bars represent the confident intervals (1.96 \times the experimental error, derived from (n) 12 injections). While no significant change is seen for $K_{d~II}$ was increased by \sim 1.9-fold when Tricine and/or phosphate buffers were used instead of Hepes.

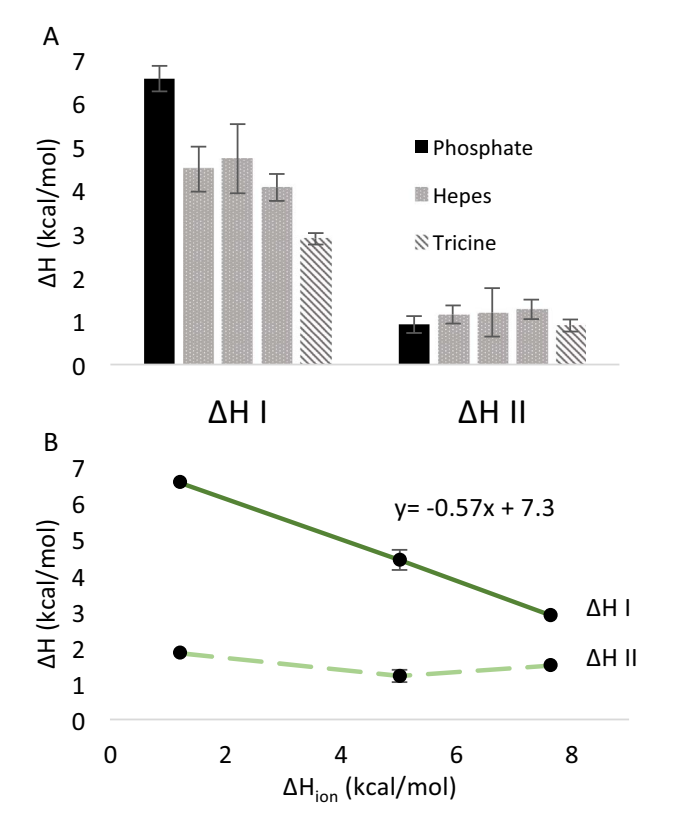


Fig. 5. Panel A, buffer effect on $\Delta H_{\rm I}$ and $\Delta H_{\rm II}$ of PSI-LHCI:Fd binding. The bars represent the confidence intervals (1.96 × the experimental error, derived from (n) 12 injections). $\Delta H_{\rm I}$ was lowest in Tricine buffer and highest in phosphate buffer while no significant change was seen for $\Delta H_{\rm II}$ values that remained steady. Panel B, dependence of ΔH to buffers' $\Delta H_{\rm ionization}$. ΔH for each buffer (the value for Hepes was a mean of three different experiments) were plotted against the specific buffer ionization enthalpy (1.22, 5.02 and 7.64 kcal/mol for phosphate, Hepes and Tricine, respectively). The gradual change in $\Delta H_{\rm II}$ corresponds to a slope of -0.57 and an intercept of 7.3 kcal/mol. $\Delta H_{\rm II}$ values were steady.

binding of Fd to PSI-LHCI are both lost in the PsaC-K35D mutant.

4. Discussion

4.1. PSI purification

This work describes the thermodynamics properties of the binding between PSI and its electron acceptor, Fd. We and others [50, 54] clearly observed two PSI populations after affinity purification of the PSI complex from C. reinhardtii. These populations correspond to PSI*

and PSI-LHCI complexes, respectively. The latter had Chl/ P_{700} ratio of 305 \pm 55 (Chl a/b of 5.7 \pm 0.6), in line with previous results from other workers [47, 52, 60–62] who reported values in the range of 207–297 Chl/ P_{700} for PSI-LHCI.

The lighter PSI population (PSI*), for which a Chl/P_{700} ratio of 106 ± 13 (Chl a/b of 24 ± 9.9) was determined, lacked not only Lhca proteins but also three core subunits (PsaF/G/K, Fig. 2). This finding is consistent with evidence that incorporation of PsaG and PsaK, following the addition of LHCI, is the last event in the assembly of the PSI-LHCI complex [54].

Those authors in [54] claimed that the immature PSI sub-complex is fully active, but we found that although PSI* is capable of Fd reduction. the overall NADP + photo-reduction activity is lower than that of PSI-LHCI by a factor of ~14. This difference can be attributed partially to the loss of PsaF, which plays an important role in the interaction between PSI and Pc [55, 56]. However, even when using DCPIP alone as the electron mediator to PSI, a marked difference was still observed: PSI* had 3.5-fold lower NADP + reduction rate (per P₇₀₀) than PSI-LHCI. Taken together, these results suggest that the two PSI complexes differ in their interaction with the terminal electron acceptor, Fd. PsaFless thylakoids from Arabidopsis were shown to have 13-fold decreased NADP + photo-reduction activity [63]. There, the authors related the lack of PsaF to destabilization in the stromal side and partial loss of PsaC/D/E. Though highly proximal, PsaF doesn't interact directly with PsaE rather through PsaA [4]. The suggestion that PsaF, when absent, is responsible for an altered Fd binding state is made, though with caution. Therefore, we hypothesized that the thermodynamics of PSI-LHCI binding to Fd would be different from that of the immature PSI* complex.

4.2. ITC results

The PSI-LHCI:Fd ITC datasets were analyzed using both the 'two sets of sites' model (Fig. 3A and Figs. S5–S6) and 'one set of sites' model (Fig. S7). To compare the different curve fittings and reject the possibility of overfitting the raw data using the two sites model, an empirical approach was taken. In all but one experiments a significant discrepancy was obtained (p < .05), in which the two-sites model clearly provided smaller distances between the observed data point, which was excluded, and the model, which was fitted without it (Fig. S9). This analysis shows that the enhanced explanatory power of the two-sites model is not an artifact caused by overfitting.

4.3. Stoichiometry

The thermogram of Fd binding to PSI-LHCI fits well as a two-component process, with each component representing a distinct binding 'event'. These events possess different enthalpies, with binding in event I being 5-15 fold tighter than in event II. Generally, two independent binding sites are represented, in an ITC curve, by $N_{\rm I}=1.0$ and $N_{\rm II}$ = 2.0, where N is the ligand to macromolecule molar ratio where site I and site II are 50% saturated, i.e. the curve's inflection points. Also, the binding curve is expected to reach saturation at a molar ratio of \sim 4 (see [64–67] for examples) giving a 2:1 stoichiometry. However, this simplified case is not applicable for PSI:Fd, as a single mutation (PsaC-K35D) was sufficient to eliminate any mode of binding. Furthermore, we obtained N value of 0.5 for event I, which may indicate that Fd was bound to two PSI-LHCI [33]. However, eukaryotic PSI is a monomer [68, 69], and it seems very unlikely that two large PSI-LHCI super-complexes (~770 kDa) [50] could ever bind a single Fd molecule (10 kDa). Another explanation for this sub-stoichiometric ratio of 0.5 could be protein heterogeneity caused by deterioration of PSI-LHCI material. This is unlikely, as all ITC experiments were conducted immediately after PSI purification and evaluation. More importantly, the very high rate of NADP + photo-reduction activity was maintained even after the ITC experiments, indicating that the super-complex is very

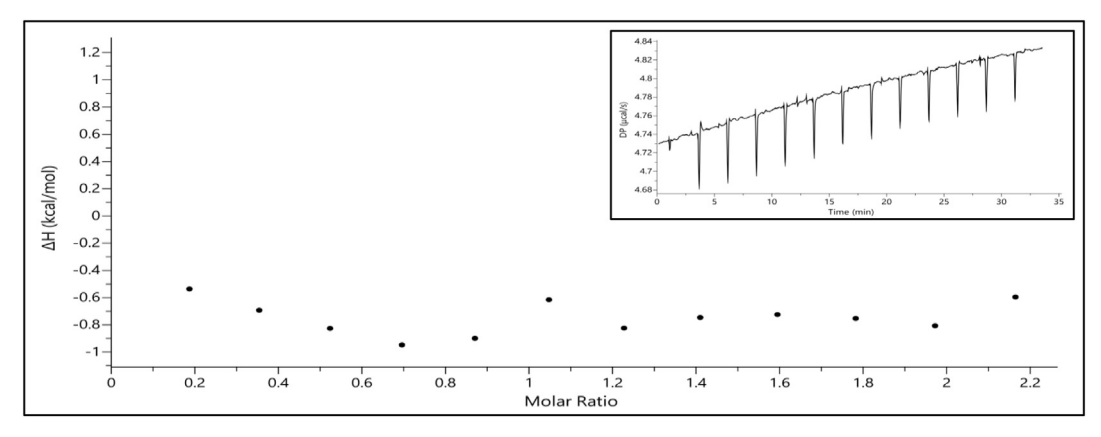


Fig. 6. Titration of PsaC K35D PSI-LHCI with Fd in Hepes buffer. The raw heat changes peaks (inset) were weak and negative indicating that there was no binding.

stable under our storage conditions. Another possibility is that after charge separation to the $P_{700}^{}(F_AF_B)^{}$ state, electron escape to oxygen forms a closed $P_{700}^{}(F_AF_B)$ state in roughly half the PSI reaction centers. This could explain the low stoichiometry for event I, if closed reaction centers (*i.e.* reduced) were unable to participate in event I. However, the P_{700} redox state is not expected to have a significant influence on Fd affinity, as P_{700} is located on the opposite side of PSI [23]. Moreover, it seems unlikely that every sample of PSI-LHCI would have happened to generate 50% closed reaction centers in such a consistent way.

Since ${\rm Mg}^{2^+}$ increases the affinity of Fd for PSI [16], another possible explanation for the odd stoichiometry is that trace amounts of divalent cations could result in PSI heterogeneity. If that was the case, a shift to one of the binding modes would have been expected in the presence of an optimal ${\rm Mg}^{2^+}$ concentration, preferably to the stronger event I. However, N and ${\rm K_d}$ values for both binding events were almost identical to those obtained without any ${\rm MgCl}_2$ (Table 2).

The possibility of thermal equilibrium between two modes of binding to the same site in PSI-LHCI was also considered. In that case, event I, the high affinity mode, is expected to be titrated first when Fd concentration is low, therefore changing the initial modes' distribution. The equilibrium would correspondingly be shifted to favor the high affinity mode. Thus, the net thermodynamic effect would be comprised of event I binding and the conformational change. The apparent K_d would then be dominated by one event, and reflected probably by a 1:1 sigmoidal curve. However, this cannot explain a bi-phasic binding curve as was repeatedly observed in our titrations. In summary, our data support a mechanism in which two binding events, sharing PsaC-Lys35, occur at a single site in PSI-LHCI. However, we could not find a satisfying explanation for the odd stoichiometry values, and this could be usefully answered in further research.

PSI* is a much simpler case. Titration of PSI* with Fd presented a sigmoidal ITC curve featuring a single binding event. The calculated stoichiometry of this event was 0.8. It should be noted that P₇₀₀ photooxidation was used to determine PSI concentration. However, it cannot distinguish between PsaF/G/K-less PSI and a complex that also lacks additional subunits that are crucial for Fd binding (for example ΔA_{705nm} during illumination were identical for PSI-LHCI and PSI* as if same amounts of P₇₀₀ were present, Fig. S1). Therefore, we can explain the low stoichiometry by the hypothesis that the PSI* pool actually consists of a mixture of immature sub-complexes, ~80% of which lack only PsaF/G/K (and LHCI) and a small population missing additional subunits. If that was the case, the actual concentration of functional PSI (i.e. capable of binding Fd) in the ITC cell would be lower and the real stoichiometry for the binding of PSI* and Fd would then be 1. It should be noted that the decrease in NADP + photo-reduction rate in the "true PSI* population" would be only 2.8-fold rather than 3.5-fold, if 20% of the population in the measurement were unable to reduce Fd.

4.4. K_d values

The K_d values determined in this investigation are lower than those observed in the past for $\it C.\ reinhardtii,\, 6–9\,\mu M\ [11–13].$ For example, we observed a $K_{d\ PSI_*}$ value of 1.5 \pm 0.23 μM for PSI*; this value is in line with values measured for higher plant PSI [25]. Although the $K_{d\ II}$ observed here for PSI-LHCI (0.2–0.4 μM) is far smaller than $K_{d\ PSI_*}$ and previously measured K_d values for the $\it C.\ reinhardtii$ PSI:Fd binding pair, it does resemble the cyanobacterial K_d of 0.2–0.6 μM seen at pH -8.0 for cyanobacterial PSI:Fd (measured by flash absorption spectroscopy) [11, 12, 14]. $K_{d\ I}$ (0.03 μM), that was observed for PSI-LHCI only in this work, is far lower than any of the previously measured K_d values under mild basic pH. Interestingly, support to such a high affinity was measured for cyanobacterial PSI:Fd at pH 5.8 [14, 19]. Another interesting observation, this time using ITC showed affinity in the nM range for titration of purified PsaD with Fd [41]. Taken together, our data suggest that a very tight association between PSI and Fd does exist.

4.5. Two Fd-binding events in mature PSI-LHCI

If one compares the binding enthalpies measured in Hepes buffer, $\Delta H_{\rm I}$ of $4.43\pm0.28\,kcal/mol$ is 3.8-fold higher than $\Delta H_{\rm II}$ (1.21 \pm 0.17 kcal/mol) and 2.5-fold higher than $\Delta H_{\rm PSI_*}$ (1.74 \pm 0.07 kcal/mol). However, $\Delta H_{\rm PSI_*}$ is only $\sim\!40\%$ higher than $\Delta H_{\rm II}$, which is a strong indication that event II and event PSI* likely represent the same binding event, perhaps with only minor differences between them. These differences may originate from conformational changes in the site or its surroundings due to the absence of PsaF/G/K and/or LHCI in PSI*. Thus, our data suggest that a fully mature algal PSI-LHCI complex has two modes for Fd binding.

Further support for the observation of two binding modes was provided by following the changes in binding enthalpy in three different buffers, but at the same pH. When the enthalpy of binding for each buffer was plotted against the buffer's intrinsic ionization enthalpy [40, 58, 59] (Fig. 5), it could be deduced that Fd binding at event I involves the net release of $\sim\!0.6$ protons on average to the solvent (n_{H+} = -0.57, Fig. 5B), while no proton uptake/release occurs at event II. The estimated K_d associated with event I, however, was not influenced by the change of buffer system (Fig. 4). Therefore, one can conclude that the binding mechanisms in operation for the two events are distinct.

4.6. The binding mechanism: entropy-driven nature of the binding

The common theme for all binding events was a positive ΔH . This means that both events are endothermic. Consequently, as both binding events are thermodynamically favorable, they must be driven by a positive change in entropy of the system. Entropy driven protein

interactions are usually attributed to hydrophobic interactions, release of water molecules or ions, and conformational changes [70–73]. It has been known for over two decades that Fd binding to PSI is facilitated by electrostatic interactions between negatively charged residues on the outer surface of Fd and positive charges on the stromal ridge of PSI [13, 23, 74]. To our surprise, Fd binding did not have a strong enthalpy component, as would have been expected from this mode of interaction. Further review of the literature provides some insights. It was shown by Canabady-Rochelle et al. (2009) and Sinn et al. (2004) that a well-defined electrostatic interaction between Ca²⁺ and polyelectrolyte [75], or between Ca²⁺ and milk proteins [76] were governed by entropy rather than enthalpy. It was suggested that an electrostatic interaction may also involve counter-ion exchange. The enthalpic contribution from such exchanges would be less exothermic than predicted simply by an electrostatic interaction [75].

The transfer of water molecules from the hydration spheres on the interaction surfaces of PSI and Fd to bulk water as the two proteins bind, however, would result in a large positive ΔS . The thermodynamic properties of Fd binding to FNR, another ET complex [77], reveal the endothermic nature of that binding [40] as well as the role of released water molecules in entropically driving the association of Fd and FNR [34, 39, 40]. Thus, the net increase in enthalpy from Fd binding to PSI is compensated by the increase in entropy from the release of water molecules and ions, resulting in a favorable interaction.

5. Conclusions

This study has confirmed that the binding of Fd to PSI follows a stoichiometry of 1 as previously argued. Also, this study has shown that there are two distinct binding events at this site, both of which are thermodynamically driven by entropy. While their associated affinities are distinct, the fact that de-protonation is involved in only one of the events supports a difference in binding mechanism. The complete elimination of any Fd binding in the PsaC-K35D mutant PSI links this residue to both binding events, consistent with the severity of this single mutation [48].

We propose a mechanism in which Fd is guided to the docking interaction with PSI in which ET takes place. Oxidized Fd approaches PsaD through electrostatic interactions and release of water molecules and proton(s). This occurs with an affinity in the nM range, in agreement with [41]; PsaC also participates in this initial docking. Following this interaction event, Fd changes its interaction mode to the final one (involving PsaE and PsaC), in which ET from the F_B cluster of PsaC to the [2Fe-2S] cluster of Fd occurs.

Transparency document

The Transparency document associated with this article can be found, in online version.

Acknowledgements

We would like to thank Prof. Nathan Nelson for fruitful discussion and suggestions.

This study was supported in part by:

- ISF iCore grant 757/12
- ISF personal grant 1646/16

Pini Marco was supported in part by a scholarship from the TAU president renewable energy center.

We would like to thank the Smoler Proteomics Center at the Technion, Israel for performing MS analysis.

We would also like to acknowledge the DNASU plasmid repository for providing the TEV protease expression plasmid used in this study.

providing the TEV protease expression plasmid used in this study. The work of Andrey Kanygin in the laboratory of Kevin Redding was

supported by NSF grant CBET-1706960 to KR.

Appendix A. Supplementary data

Supplementary data to this article can be found online at https://doi.org/10.1016/j.bbabio.2018.01.001.

References

- [1] W. Junge, N. Nelson, ATP synthase, Annu. Rev. Biochem. 84 (2015) 631-657.
- [2] A.M. Terauchi, S.F. Lu, M. Zaffagnini, S. Tappa, M. Hirasawa, J.N. Tripathy, D.B. Knaff, P.J. Farmer, S.D. Lemaire, T. Hase, S.S. Merchant, Pattern of expression and substrate specificity of chloroplast ferredoxins from *Chlamydomonas reinhardtii*, J. Biol. Chem. 284 (2009) 25867–25.878.
- [3] T. Hase, P. Schürmann, D.B. Knaff, The interaction of ferredoxin with ferredoxindependent enzymes, in: J.H. Golbeck (Ed.), Photosystem I: The Light-Driven Plastocyanin:Ferredoxin Oxidoreductase, Springer Netherlands, Dordrecht, 2006, pp. 477–498.
- [4] Y. Mazor, A. Borovikova, N. Nelson, The Structure of plant photosystem I supercomplex at 2.8A resolution, Nat. Plants 3 (2017) (17014-17014).
- [5] M.G. Muller, C. Slavov, R. Luthra, K.E. Redding, A.R. Holzwarth, Independent initiation of primary electron transfer in the two branches of the photosystem I reaction center, Proc. Natl. Acad. Sci. U. S. A. 107 (2010) 4123–4128.
- [6] G. Hanke, P. Mulo, Plant type ferredoxins and ferredoxin-dependent metabolism, Plant Cell Environ. 36 (2013) 1071–1084.
- [7] M. Winkler, A. Hemschemeier, J. Jacobs, S. Stripp, T. Happe, Multiple ferredoxin isoforms in *Chlamydomonas reinhardtii* - their role under stress conditions and biotechnological implications, Eur. J. Cell Biol. 89 (2010) 998–1004.
- [8] A. Díaz-Quintana, W. Leibl, H. Bottin, P. Sétif, Electron transfer in photosystem I reaction centers follows a linear pathway in which iron—sulfur cluster FB is the immediate electron donor to soluble ferredoxin, Biochemistry 37 (1998) 3429—3439
- [9] A.A. Mamedova, M.D. Mamedov, K.N. Gourovskaya, I.R. Vassiliev, J.H. Golbeck, A.Y. Semenov, Electrometrical study of electron transfer from the terminal FA/FB iron-sulfur clusters to external acceptors in photosystem I, FEBS Lett. 462 (1999) 421–424.
- [10] I.R. Vassiliev, Y.-S. Jung, F. Yang, J.H. Golbeck, PsaC subunit of photosystem I is oriented with iron-sulfur cluster FB as the immediate electron donor to ferredoxin and flavodoxin, Biophys. J. 74 (1998) 2029–2035.
- [11] N. Fischer, P. Setif, J.D. Rochaix, Targeted mutations in the psaC gene of Chlamydomonas reinhardtii: preferential reduction of FB at low temperature is not accompanied by altered electron flow from photosystem I to ferredoxin, Biochemistry 36 (1997) 93–102.
- [12] N. Fischer, P. Setif, J.D. Rochaix, Site-directed mutagenesis of the PsaC subunit of photosystem I. F(b) is the cluster interacting with soluble ferredoxin, J. Biol. Chem. 274 (1999) 23333–23,340.
- [13] P. Setif, Ferredoxin and flavodoxin reduction by photosystem I, Biochim. Biophys. Acta 1507 (2001) 161–179.
- [14] P.Q. Setif, H. Bottin, Laser flash absorption spectroscopy study of ferredoxin reduction by photosystem I: spectral and kinetic evidence for the existence of several photosystem I-ferredoxin complexes, Biochemistry 34 (1995) 9059–9070.
- [15] C. Jolley, A. Ben-Shem, N. Nelson, P. Fromme, Structure of plant photosystem I revealed by theoretical modeling, J. Biol. Chem. 280 (2005) 33627–33636.
- [16] P.Q. Setif, H. Bottin, Laser flash absorption spectroscopy study of ferredoxin reduction by photosystem I in Synechocystis sp. PCC 6803: evidence for submicrosecond and microsecond kinetics, Biochemistry 33 (1994) 8495–8504.
- [17] P. Barth, I. Guillouard, P. Setif, B. Lagoutte, Essential role of a single arginine of photosystem I in stabilizing the electron transfer complex with ferredoxin, J. Biol. Chem. 275 (2000) 7030–7036.
- [18] J. Hanley, P. Setif, H. Bottin, B. Lagoutte, Mutagenesis of photosystem I in the region of the ferredoxin cross-linking site: modifications of positively charged amino acids, Biochemistry 35 (1996) 8563–8571.
- [19] P. Barth, B. Lagoutte, P. Setif, Ferredoxin reduction by photosystem I from Synechocystis sp. PCC 6803: toward an understanding of the respective roles of subunits PsaD and PsaE in ferredoxin binding, Biochemistry 37 (1998) 16233–16.241.
- [20] J. Janin, The kinetics of protein-protein recognition, Proteins 28 (1997) 153-161.
- [21] G. Schreiber, A.R. Fersht, Rapid, electrostatically assisted association of proteins, Nat. Struct. Biol. 3 (1996) 427–431.
- [22] C. Mignee, R. Mutoh, A. Krieger-Liszkay, G. Kurisu, P. Setif, Gallium ferredoxin as a tool to study the effects of ferredoxin binding to photosystem I without ferredoxin reduction, Photosynth. Res. 134 (3) (2017) 251–263.
- [23] P. Setif, N. Harris, B. Lagoutte, S. Dotson, S.R. Weinberger, Detection of the photosystem I:ferredoxin complex by backscattering interferometry, J. Am. Chem. Soc. 132 (2010) 10620–10.622.
- [24] O. Klukas, W.D. Schubert, P. Jordan, N. Krauss, P. Fromme, H.T. Witt, W. Saenger, Photosystem I, an improved model of the stromal subunits PsaC, PsaD, and PsaE, J. Biol. Chem. 274 (1999) 7351–7360.
- [25] S.V. Ruffle, A.O. Mustafa, A. Kitmitto, A. Holzenburg, R.C. Ford, The location of the mobile electron carrier ferredoxin in vascular plant photosystem I, J. Biol. Chem. 275 (2000) 36250–36,255.
- [26] D.J. Cashman, T. Zhu, R.F. Simmerman, C. Scott, B.D. Bruce, J. Baudry, Molecular interactions between photosystem I and ferredoxin: an integrated energy frustration

- and experimental model, J. Mol. Recognit. 27 (2014) 597-608.
- [27] I. Lee, J.W. Lee, A. Stubna, E. Greenbaum, Measurement of electrostatic potentials above oriented single photosynthetic reaction centers, J. Phys. Chem. B 104 (2000) 2439–2443.
- [28] M. Jenik, R.G. Parra, L.G. Radusky, A. Turjanski, P.G. Wolynes, D.U. Ferreiro, Protein frustratometer: a tool to localize energetic frustration in protein molecules, Nucleic Acids Res. 40 (2012) W348–351.
- [29] B. Andersen, H.V. Scheller, B.L. Moller, The PSI-E subunit of photosystem I binds ferredoxin:NADP+ oxidoreductase, FEBS Lett. 311 (1992) 169–173.
- [30] J.J. van Thor, T.H. Geerlings, H.C. Matthijs, K.J. Hellingwerf, Kinetic evidence for the PsaE-dependent transient ternary complex photosystem I/Ferredoxin/Ferredoxin:NADP(+) reductase in a cyanobacterium, Biochemistry 38 (1999) 12735–12,746.
- [31] J.J. van Thor, Light Harvesting and State Transitions in Cyanobacteria, 111 (1998), pp. 430–443.
- [32] I. Yacoby, S. Pochekailov, H. Toporik, M.L. Ghirardi, P.W. King, S. Zhang, Photosynthetic electron partitioning between [FeFe]-hydrogenase and ferredoxin:NADP+-oxidoreductase (FNR) enzymes in vitro, Proc. Natl. Acad. Sci. U. S. A. 108 (2011) 9396–9401.
- [33] H. Fernando, C. Chin, J. Rosgen, K. Rajarathnam, Dimer dissociation is essential for interleukin-8 (IL-8) binding to CXCR1 receptor, J. Biol. Chem. 279 (2004) 36175–36.178.
- [34] L. Piubelli, G. Zanetti, H.R. Bosshard, Recombinant wild-type and mutant complexes of ferredoxin and ferredoxin:NADP+ reductase studied by isothermal titration calorimetry, Biol. Chem. 378 (1997) 715–718.
- [35] K. Rajarathnam, J. Rosgen, Isothermal titration calorimetry of membrane proteins progress and challenges, Biochim. Biophys. Acta 1838 (2014) 69–77.
- [36] S. Vega, O. Abian, A. Velazquez-Campoy, On the link between conformational changes, ligand binding and heat capacity, Biochim. Biophys. Acta 1860 (2016) 868–878
- [37] V. Linkuviene, G. Krainer, W.Y. Chen, D. Matulis, Isothermal titration calorimetry for drug design: precision of the enthalpy and binding constant measurements and comparison of the instruments, Anal. Biochem. 515 (2016) 61–64.
- [38] K. Zimmermann, M. Heck, J. Frank, J. Kern, I. Vass, A. Zouni, Herbicide binding and thermal stability of photosystem II isolated from *Thermosynechococcus elon*gatus, Biochim. Biophys. Acta 1757 (2006) 106–114.
- [39] I. Jelesarov, H.R. Bosshard, Thermodynamics of ferredoxin binding to ferredoxin:NADP+ reductase and the role of water at the complex interface, Biochemistry 33 (1994) 13321–13,328.
- [40] M. Martinez-Julvez, M. Medina, A. Velazquez-Campoy, Binding thermodynamics of ferredoxin:NADP+ reductase: two different protein substrates and one energetics, Biophys. J. 96 (2009) 4966–4975.
- [41] P. Jin, J. Sun, P.R. Chitnis, Structural features and assembly of the soluble overexpressed PsaD subunit of photosystem I, Biochim. Biophys. Acta 1410 (1999) 7–18.
- [42] F.W. Studier, Protein production by auto-induction in high density shaking cultures, Protein Expr. Purif. 41 (2005) 207–234.
- [43] P.G. Blommel, B.G. Fox, A combined approach to improving large-scale production of tobacco etch virus protease, Protein Expr. Purif. 55 (2007) 53–68.
- [44] O. Ben Zvi, I. Yacoby, The in-vitro enhancement of FeFe hydrogenase activity by superoxide dismutase, Int. J. Hydrog. Energy 41 (2016) 17274–17,282.
- [45] N. Cassan, B. Lagoutte, P. Sétif, Ferredoxin-NADP+ reductase: kinetics of electron transfer, transient intermediates, and catalytic activities studied by flash-absorption spectroscopy with isolated photosystem I and ferredoxin, J. Biol. Chem. 280 (2005) 25960–25, 972.
- [46] M. Shin, [40] Ferredoxin-NADP reductase from spinach, Methods Enzymol. 23 (1971) 440-447.
- [47] G. Gulis, K.V. Narasimhulu, L.N. Fox, K.E. Redding, Purification of His6-tagged Photosystem I from Chlamydomonas reinhardtii, Photosynth. Res. 96 (2008) 51–60.
- [48] N. Fischer, M. Hippler, P. Setif, J.P. Jacquot, J.D. Rochaix, The PsaC subunit of photosystem I provides an essential lysine residue for fast electron transfer to ferredoxin, EMBO J. 17 (1998) 849–858.
- [49] R.J. Porra, The chequered history of the development and use of simultaneous equations for the accurate determination of chlorophylls a and b, Photosynth. Res. 73 (2002) 149–156.
- [50] B. Drop, M. Webber-Birungi, F. Fusetti, R. Kouril, K.E. Redding, E.J. Boekema, R. Croce, Photosystem I of *Chlamydomonas reinhardtii* contains nine light-harvesting complexes (Lhca) located on one side of the core, J. Biol. Chem. 286 (2011) 44878–44.887.
- [51] J. Cox, M. Mann, MaxQuant enables high peptide identification rates, individualized p.p.b.-range mass accuracies and proteome-wide protein quantification, Nat. Biotechnol. 26 (2008) 1367–1372.
- [52] H. Witt, E. Bordignon, D. Carbonera, J.P. Dekker, N. Karapetyan, C. Teutloff, A. Webber, W. Lubitz, E. Schlodder, Species-specific differences of the spectroscopic properties of P700: analysis of the influence of non-conserved amino acid residues by site-directed mutagenesis of photosystem I from *Chlamydomonas reinhardtii*, J. Biol. Chem. 278 (2003) 46760–46,771.

- [53] G. Wittenberg, S. Jarvi, M. Hojka, S.Z. Toth, E.H. Meyer, E.M. Aro, M.A. Schottler, R. Bock, Identification and characterization of a stable intermediate in photosystem I assembly in tobacco, Plant J. 90 (2017) 478–490.
- [54] S. Ozawa, T. Onishi, Y. Takahashi, Identification and characterization of an assembly intermediate subcomplex of photosystem I in the green alga *Chlamydomonas* reinhardtii, J. Biol. Chem. 285 (2010) 20072–20079.
- [55] J. Farah, F. Rappaport, Y. Choquet, P. Joliot, J.D. Rochaix, Isolation of a psaf-deficient mutant of Chlamydomonas reinhardtii: efficient interaction of plastocyanin with the photosystem I reaction center is mediated by the PsaF subunit, EMBO J. 14 (1995) 4976–4984.
- [56] M. Hippler, J. Reichert, M. Sutter, E. Zak, L. Altschmied, U. Schröer, R.G. Herrmann, W. Haehnel, The plastocyanin binding domain of photosystem I, EMBO J. 15 (1996) 6374–6384.
- [57] A.B. Wohri, P. Hillertz, P.O. Eriksson, J. Meuller, N. Dekker, A. Snijder, Thermodynamic studies of ligand binding to the human homopentameric glycine receptor using isothermal titration calorimetry, Mol. Membr. Biol. 30 (2013) 169-183
- [58] H. Fukada, K. Takahashi, Enthalpy and heat capacity changes for the proton dissociation of various buffer components in 0.1 M potassium chloride, Proteins 33 (1998) 159–166.
- [59] B.M. Baker, K.P. Murphy, Evaluation of linked protonation effects in protein binding reactions using isothermal titration calorimetry, Biophys. J. 71 (1996) 2049–2055.
- [60] B. Drop, K.N.S. Yadav, E.J. Boekema, R. Croce, Consequences of state transitions on the structural and functional organization of photosystem I in the green alga *Chlamydomonas reinhardtii*, Plant J. 78 (2014) 181–191.
- [61] C. Le Quiniou, B. van Oort, B. Drop, I.H. van Stokkum, R. Croce, The high efficiency of photosystem i in the green alga *Chlamydomonas reinhardtii* is maintained after the antenna size is substantially increased by the association of light-harvesting complexes II, J. Biol. Chem. 290 (2015) 30587–30,595.
- [62] H. Takahashi, A. Okamuro, J. Minagawa, Y. Takahashi, Biochemical characterization of photosystem I-associated light-harvesting complexes I and II isolated from state 2 cells of *Chlamydomonas reinhardtii*, Plant Cell Physiol. 55 (2014) 1437–1449.
- [63] A. Haldrup, D.J. Simpson, H.V. Scheller, Down-regulation of the PSI-F subunit of photosystem I (PSI) in *Arabidopsis thaliana*. The PSI-F subunit is essential for photoautotrophic growth and contributes to antenna function, J. Biol. Chem. 275 (2000) 31211–31,218.
- [64] J.D. Eaton, M.P. Williamson, Multi-site binding of epigallocatechin gallate to human serum albumin measured by NMR and isothermal titration calorimetry, Biosci. Rep. 37 (2017).
- [65] I. Gorshkova, J.L. Moore, K.H. McKenney, F.P. Schwarz, Thermodynamics of cyclic nucleotide binding to the cAMP receptor protein and its T127L mutant, J. Biol. Chem. 270 (1995) 21679–21.683.
- [66] M. Harty, S. Bearne, Measuring benzohydroxamate complexation with Mg, Mn, Co, and Ni using isothermal titration calorimetry, J. Therm. Anal. Calorim. 123 (2016) 2573–2582.
- [67] S. Lee, Y.C. Tsai, R. Mattera, W.J. Smith, M.S. Kostelansky, A.M. Weissman, J.S. Bonifacino, J.H. Hurley, Structural basis for ubiquitin recognition and autoubiquitination by Rabex-5, Nat. Struct. Mol. Biol. 13 (2006) 264–271.
- [68] E.J. Boekema, P.E. Jensen, E. Schlodder, J.F.L. van Breemen, H. van Roon, H.V. Scheller, J.P. Dekker, Green plant photosystem I binds light-harvesting complex I on one side of the complex, Biochemistry 40 (2001) 1029–1036.
- [69] R. Kouril, N. van Oosterwijk, A.E. Yakushevska, E.J. Boekema, Photosystem I: a search for green plant trimers, Photochem. Photobiol. Sci. 4 (2005) 1091–1094.
- [70] B. Baum, L. Muley, M. Smolinski, A. Heine, D. Hangauer, G. Klebe, Non-additivity of functional group contributions in protein-ligand binding: a comprehensive study by crystallography and isothermal titration calorimetry, J. Mol. Biol. 397 (2010) 1042–1054.
- [71] G.P. Brady, K.A. Sharp, Entropy in protein folding and in protein-protein interactions, Curr. Opin. Struct. Biol. 7 (1997) 215–221.
- [72] J.D. Chodera, D.L. Mobley, Entropy-enthalpy compensation: role and ramifications in biomolecular ligand recognition and design, Annu. Rev. Biophys. 42 (2013) 121–142.
- [73] F. Guerlesquin, J.C. Sari, M. Bruschi, Thermodynamic parameters of cytochrome c3-ferredoxin complex formation, Biochemistry 26 (1987) 7438–7443.
- [74] P. Setif, N. Fischer, B. Lagoutte, H. Bottin, J.D. Rochaix, The ferredoxin docking site of photosystem I, Biochim. Biophys. Acta 1555 (2002) 204–209.
- [75] C.G. Sinn, R. Dimova, M. Antonietti, Isothermal titration calorimetry of the polyelectrolyte/water interaction and binding of Ca2+: effects determining the quality of polymeric scale inhibitors, Macromolecules 37 (2004) 3444–3450.
- [76] L.S. Canabady-Rochelle, C. Sanchez, M. Mellema, S. Banon, Study of calcium-soy protein interactions by isothermal titration calorimetry and pH cycle, J. Agric. Food Chem. 57 (2009) 5939–5947.
- [77] J.K. Hurley, G. Tollin, M. Medina, C. Gómez-Moreno, Electron transfer from ferredoxin and flavodoxin to ferredoxin:NADP + reductase, in: J.H. Golbeck (Ed.), Photosystem I: The Light-Driven Plastocyanin:Ferredoxin Oxidoreductase, Springer Netherlands, Dordrecht, 2006, pp. 455–476.